



 Cite this: *RSC Adv.*, 2026, 16, 11246

# Pseudo-two-dimensional multiphysics modeling of mass transport and pseudo-enzymatic kinetics in $\text{Ti}_3\text{C}_2\text{T}_x\text{@Pt}$ MXene-based glucose biosensors

 Mohamed Abu Shuheil,<sup>a</sup> Thamer Hani,<sup>b</sup> Roopashree R,<sup>c</sup> Subhashree Ray,<sup>d</sup> Baraa Mohammed Yaseen,<sup>e</sup> Kavitha V,<sup>f</sup> Renu Sharma,<sup>g</sup> Aashna Sinha<sup>h</sup> and Amir Arsalanirad \*<sup>i</sup>

Accurate glucose sensing in nanozyme-based platforms is fundamentally governed by the coupled interplay between mass transport and surface-confined catalytic reactions, particularly in systems characterized by intrinsic nanoscale heterogeneity. In this work, a pseudo-two-dimensional (pseudo-2D) multiphysics modeling framework is developed to elucidate diffusion-reaction interactions in  $\text{Ti}_3\text{C}_2\text{T}_x\text{@Pt}$  MXene-based glucose biosensors by explicitly resolving two-dimensional diffusion of glucose and hydrogen peroxide in the electrolyte while confining pseudo-enzymatic reactions to laterally heterogeneous Pt catalytic domains described by Michaelis–Menten kinetics. The simulations demonstrate that non-uniform Pt site distributions induce pronounced local substrate depletion, lateral concentration gradients, and an effective thickening of the diffusion layer, resulting in transport bottlenecks that are not captured by conventional one-dimensional models. As a consequence, the pseudo-2D framework predicts a systematic reduction in effective glucose flux, premature saturation of the sensor response, and significant shifts in apparent kinetic parameters, including an increased effective Michaelis constant and a decreased maximum reaction rate, despite identical mean catalyst loading. In addition, the model reveals enhanced accumulation and delayed transport of hydrogen peroxide within the diffusion layer, directly modulating colorimetric signal intensity and response dynamics. Quantitative comparison with experimentally reported UV-vis absorbance spectra and electrochemical response trends shows excellent agreement across physiologically relevant glucose concentrations, confirming the predictive capability of the proposed approach. Overall, these findings highlight the critical role of lateral catalyst dispersion in governing mass transport limitations, apparent kinetics, and sensing performance, and establish the pseudo-2D multiphysics framework as a computationally efficient and physically rigorous tool for the rational design and optimization of heterogeneous MXene nanozyme-based glucose biosensors.

Received 19th December 2025

Accepted 14th February 2026

DOI: 10.1039/d5ra09807f

[rsc.li/rsc-advances](https://rsc.li/rsc-advances)
<sup>a</sup>Faculty of Allied Medical Sciences, Hourani Center for Applied Scientific Research, Al-Ahliyya Amman University, Amman, Jordan

<sup>b</sup>Department of Dental Medicine, College of Dental Medicine, AL-Turath University, Baghdad, Iraq

<sup>c</sup>Department of Chemistry and Biochemistry, School of Sciences, JAIN (Deemed to be University), Bangalore, Karnataka, India

<sup>d</sup>Department of Biochemistry, IMS and SUM Hospital, Siksha 'O' Anusandhan, Bhubaneswar, Odisha-751003, India

<sup>e</sup>Department of Medical Laboratory Technics, College of Health and Medical Technology, Alnoor University, Mosul, Iraq

<sup>f</sup>Department of Chemistry, Sathyabama Institute of Science and Technology, Chennai, Tamil Nadu, India

<sup>g</sup>Department of Chemistry, University Institute of Sciences, Chandigarh University, Mohali, Punjab, India

<sup>h</sup>School of Applied and Life Sciences, Division of Research and Innovation, Uttarakhand University, Dehradun, Uttarakhand, India

<sup>i</sup>Young Researchers and Elite Club, Islamic Azad University of Tehran, Tehran, Iran. E-mail: amirarsalaniradacademic@gmail.com

## 1. Introduction

Understanding and optimizing glucose sensing mechanisms remain central to advancing biosensor technologies for clinical diagnostics and health monitoring. Accurate glucose detection is essential in managing metabolic disorders, particularly diabetes mellitus, which continues to present significant global health challenges.<sup>1</sup> Among the diverse strategies explored, nanozyme-based sensors (artificial enzyme mimetics exhibiting catalytic functionalities) have emerged as robust alternatives to natural enzymes due to their enhanced stability, tunable activity, and cost-effectiveness.<sup>2–4</sup> Peroxidase-like (POD) nanozymes, especially, catalyze the decomposition of hydrogen peroxide ( $\text{H}_2\text{O}_2$ ) and generate detectable signals *via* colorimetric, electrochemical, or chemiluminescent pathways.<sup>5,6</sup> This attribute underlies their broad application in biosensing, including glucose analysis, where glucose oxidase ( $\text{GO}_x$ )



catalyzes glucose oxidation to gluconic acid and  $\text{H}_2\text{O}_2$ , which is subsequently processed by the nanozyme.<sup>7</sup>

Two-dimensional (2D) transition metal carbides/nitrides (MXenes) (particularly  $\text{Ti}_3\text{C}_2\text{T}_x$ ) represent a transformative class of materials in nanozyme design and advanced biosensing due to their high conductivity, large surface area, hydrophilic surface terminations, and facile surface functionalization.<sup>8,9</sup> These features promote efficient electron transport and abundant active sites, which are key for enhancing catalytic efficiency and lowering detection limits.<sup>10,11</sup> MXene-based composites integrated with noble metal nanoparticles (*e.g.*, Pt, Au) have shown remarkable peroxidase-like activity and improved electrochemical responses for glucose detection, achieving wide linear ranges and low limits of detection (LOD).<sup>12,13</sup>

Despite these material advances, sensor performance is fundamentally governed by mass transport dynamics and heterogeneous catalytic interactions at the nanozyme interface. Traditional modeling techniques often employ one-dimensional (1D) assumptions of homogeneous surfaces and uniform activity,<sup>14</sup> which inadequately capture the complex interplay between lateral heterogeneity of active sites, diffusion gradients, and reaction kinetics. Recent reports emphasize that non-uniform distributions of catalytic clusters and nanozyme morphology can drastically influence substrate accessibility and effective kinetic parameters, highlighting the limitations of simplified models in predicting sensor behavior.<sup>15,16</sup>

To bridge this gap, multiphysics modeling approaches have been developed to resolve coupled mass transport and surface reaction phenomena in more realistic geometries.<sup>17–19</sup> For example, mesoscopic studies integrating microkinetic frameworks and transport effects elucidate how catalyst roughness and lateral heterogeneities affect selectivity and reaction pathways in related electrocatalytic systems.<sup>20</sup> Extending such modeling to nanozyme-based glucose sensing platforms offers critical insight into how diffusion-limited transport and pseudo-enzymatic kinetics collectively govern sensor outputs, such as apparent Michaelis–Menten constants ( $K_m$ ) and maximum reaction rates.<sup>21,22</sup>

The pseudo-two-dimensional (pseudo-2D) multiphysics model adopted here explicitly accounts for diffusion in both lateral and vertical directions above a heterogeneous  $\text{Ti}_3\text{C}_2\text{T}_x$ @Pt nanozyme-modified surface.<sup>23</sup> By confining catalytic reactions to the solid–liquid boundary and allowing two-dimensional diffusion in the overlying domain, the model effectively captures surface clustering effects without resorting to computationally expensive full 3D simulations. Such an approach has been shown to reveal significant deviations in mass transport profiles, effective diffusion layer thickness, and aggregated kinetic behavior compared to traditional 1D formulations.<sup>24–26</sup> These deviations are especially pronounced when lateral gradients, induced by heterogeneous distributions of active Pt sites, give rise to transport-controlled flux limitation and substrate depletion “hot-spots” that reduce effective substrate availability at the nanozyme surface.

Furthermore, integrating realistic  $\text{H}_2\text{O}_2$  transport and consumption dynamics is essential for colorimetric response prediction, as intermediate buildup and delayed outward

diffusion contribute to signal modulation.<sup>27–29</sup> Similarly, electrochemical reactions (involving direct glucose oxidation at the electrode interface) are sensitive to catalytic site density and transport-limited flux, affecting overall current responses.<sup>30–32</sup> Consequently, pseudo-2D frameworks that account for spatially varying surface reactivity provide a more accurate mechanistic basis for interpreting experimental calibration curves and for guiding optimization strategies based on nanozyme dispersion and morphology.

In this work, a pseudo-two-dimensional (pseudo-2D) multiphysics model is developed to quantitatively investigate the role of lateral surface heterogeneity on mass transport and pseudo-enzymatic kinetics in a  $\text{Ti}_3\text{C}_2\text{T}_x$ @Pt nanozyme-based glucose sensing platform. The model, implemented in COMSOL Multiphysics, explicitly couples two-dimensional diffusion of glucose and hydrogen peroxide in the electrolyte with surface-confined Michaelis–Menten reaction kinetics at spatially heterogeneous catalytic domains. Key parameters, including Pt cluster size, inter-cluster spacing, surface coverage, diffusion layer thickness, apparent ( $K_m$ ), and effective reaction rates, are systematically evaluated. By comparing pseudo-2D predictions with conventional 1D formulations and experimental calibration data, this study aims to elucidate how nanoscale catalyst distribution governs effective kinetic parameters and sensor sensitivity, thereby providing a predictive framework for the rational design and optimization of high-performance nanozyme-based glucose biosensors.

## 2. Methodology

The development of nanozyme-based biosensors for glucose detection relies on the intricate interplay between mass transport phenomena and surface-catalyzed reactions. In this study, a pseudo-two-dimensional (pseudo-2D) multiphysics model is formulated to describe the mass transport and pseudo-enzymatic kinetics of glucose and hydrogen peroxide ( $\text{H}_2\text{O}_2$ ) in the vicinity of  $\text{Ti}_3\text{C}_2\text{T}_x$ @Pt MXene nanozymes, as employed in the dual-mode colorimetric and electrochemical glucose detection platform. This modeling approach captures the essential features of heterogeneous surface catalysis while maintaining computational efficiency, making it suitable for elucidating the influence of Pt nanoparticle distribution on sensor performance.

### 2.1. Pseudo-2D geometry

The computational domain is defined as a rectangular two-dimensional region that represents the diffusion layer adjacent to the  $\text{Ti}_3\text{C}_2\text{T}_x$ @Pt-modified electrode surface. The horizontal dimension (*x*-direction) spans a length *L*, which corresponds to a representative segment of the electrode surface, incorporating variations in the local density and distribution of Pt nanoparticles supported on the  $\text{Ti}_3\text{C}_2\text{T}_x$  MXene sheets. The vertical dimension (*y*-direction) extends from *y* = 0 (the active surface) to *y* = *H* (the bulk solution boundary), where *H* denotes the thickness of the diffusion layer.



The lower boundary at  $y = 0$  represents the  $\text{Ti}_3\text{C}_2\text{T}_x\text{@Pt}$  nanocomposite surface, where pseudo-enzymatic reactions occur exclusively. The upper boundary at  $y = H$  interfaces with the well-stirred bulk solution, maintaining constant analyte concentrations. Lateral boundaries at  $x = 0$  and  $x = L$  are treated as symmetry or no-flux conditions to simulate periodic repetition of the surface features. This pseudo-2D formulation approximates the three-dimensional complexity of the nanocomposite surface by confining reactions to the  $y = 0$  boundary while allowing two-dimensional diffusion in the overlying solution layer. The geometry strikes a balance between capturing lateral heterogeneities in catalytic activity and avoiding the prohibitive computational cost of full three-dimensional simulations.

## 2.2. Physics interfaces

The model integrates two primary physics modules: (i) Transport of diluted species in the bulk domain (2D) and (ii) surface reactions at the active boundary. Convection is neglected, as the system operates under quiescent conditions typical of colorimetric assays and chronoamperometric electrochemical measurements, rendering diffusion the dominant transport mechanism. Electrostatic effects and migration are omitted, given the neutral or buffered electrolyte environments used in the experimental protocols.

The species tracked include glucose (Glu) and hydrogen peroxide ( $\text{H}_2\text{O}_2$ ), the latter being both a product of enzymatic glucose oxidation and a substrate for the peroxidase-like activity of the  $\text{Ti}_3\text{C}_2\text{T}_x\text{@Pt}$  nanozyme. For colorimetric simulations, the oxidation of 3,3',5,5'-tetramethylbenzidine (TMB) is implicitly incorporated through the  $\text{H}_2\text{O}_2$  consumption rate, whereas electrochemical simulations focus on direct electrooxidation of glucose at the modified electrode.

## 2.3. Governing equations

The pseudo-two-dimensional multiphysics model describes the diffusion-dominated transport of glucose (Glu) and hydrogen peroxide ( $\text{H}_2\text{O}_2$ ) in the solution domain overlying the heterogeneous  $\text{Ti}_3\text{C}_2\text{T}_x\text{@Pt}$  surface, coupled with surface-confined pseudo-enzymatic reactions. Mass transport for each species  $i$  ( $i = \text{Glu}, \text{H}_2\text{O}_2$ ) is governed by Fick's second law in the two-dimensional domain 33:

$$\frac{\partial C_i}{\partial t} = D_i \left( \frac{\partial^2 C_i}{\partial x^2} + \frac{\partial^2 C_i}{\partial y^2} \right) \quad (1)$$

where  $C_i(x, y, t)$  denotes the local concentration,  $t$  is time, and  $D_i$  is the diffusion coefficient ( $D_{\text{Glu}} = 6.7 \times 10^{-10} \text{ m}^2 \text{ s}^{-1}$ ;  $D_{\text{H}_2\text{O}_2} = 1.5 \times 10^{-9} \text{ m}^2 \text{ s}^{-1}$ ). This equation applies throughout the rectangular domain ( $0 \leq x \leq L$ ,  $0 \leq y \leq H$ ), assuming dilute-solution conditions and negligible convective or migrative contributions, consistent with quiescent experimental setups in both colorimetric and chronoamperometric protocols.<sup>34</sup>

The pseudo-2D approximation is invoked by the scale separation inherent to the system: lateral gradients are significantly weaker than vertical ones in the bulk of the diffusion layer, *i.e.*,  $|\partial C_i / \partial x| \ll |\partial C_i / \partial y|$ , except in close proximity to the heterogeneous

boundary where localized Pt nanoparticle clusters induce modest  $x$ -directional variations. This enables retention of two-dimensional diffusion while confining catalytic reactions exclusively to the  $y = 0$  boundary, avoiding the computational demands of fully three-dimensional heterogeneous modeling.

At the reactive surface ( $y = 0$ ), diffusive flux from the solution phase is balanced by the heterogeneous reaction rate:

$$-D_i \left. \frac{\partial C_i}{\partial y} \right|_{y=0} = R_i(C_{i,s}) \quad (2)$$

where  $C_{i,s}(x, t) = C_i(x, 0, t)$  is the surface concentration, and  $R_i$  represents the net consumption (for substrates) or production rate. The peroxidase-like activity of  $\text{Ti}_3\text{C}_2\text{T}_x\text{@Pt}$ , primarily attributed to Pt sites, is described by Michaelis–Menten kinetics for  $\text{H}_2\text{O}_2$  consumption in the colorimetric mode:<sup>35</sup>

$$R_{\text{H}_2\text{O}_2} = -\frac{V_{\text{max}} \Gamma_{\text{Pt}}(x) C_{\text{H}_2\text{O}_2,s}}{K_m + C_{\text{H}_2\text{O}_2,s}} \quad (3)$$

With  $V_{\text{max}}$  the maximum turnover frequency per active site,  $K_m$  the intrinsic Michaelis constant ( $\sim 2.5 \text{ mM}$ , derived from homogeneous Pt benchmarks adjusted for nanozyme behavior), and  $\Gamma_{\text{Pt}}(x)$  the local surface site density, parameterized sinusoidally (50% amplitude variation around the mean) to emulate clustering observed in TEM/EDS mappings.<sup>34</sup> Upstream  $\text{H}_2\text{O}_2$  production from glucose oxidase (GOD)-catalyzed glucose oxidation is incorporated as a source term:

$$R_{\text{H}_2\text{O}_2} = k_{\text{GOD}} C_{\text{Glu},s} \quad (4)$$

where  $k_{\text{GOD}}$  is an effective first-order rate constant calibrated to experimental incubation conditions.

For direct glucose electrooxidation in the electrochemical mode, an analogous heterogeneous Michaelis–Menten form is adopted:<sup>35</sup>

$$R_{\text{Glu}} = -\frac{V_{\text{max,el}} \Gamma_{\text{Pt}}(x) C_{\text{Glu},s}}{K_{\text{m,el}} + C_{\text{Glu},s}} \quad (5)$$

With parameters  $V_{\text{max,el}}$  and  $K_{\text{m,el}}$  tuned to chronoamperometric responses. To extract observable macroscopic quantities comparable to experimental data, spatial averaging along the  $x$ -direction is performed:

$$\bar{C}_i(y, t) = \frac{1}{L} \int_0^L C_i(x, y, t) dx \quad (6)$$

Yielding effective one-dimensional profiles. Similarly, the effective surface concentration  $C_{i,s}^{\text{eff}}(t) = \bar{C}_i(0, t)$  and effective flux  $J_{\text{eff}}(t) = \frac{1}{L} \int_0^L \left[ -D_i \left. \frac{\partial C_i}{\partial y} \right|_{y=0} \right] dx$  enable fitting of apparent kinetic parameters ( $K_m^{\text{eff}}, V_{\text{max}}^{\text{eff}}$ ) *via*:<sup>36</sup>

$$R_{\text{eff}} = J_{\text{eff}} = \frac{V_{\text{max}}^{\text{eff}} C_{i,s}^{\text{eff}}}{K_m^{\text{eff}} + C_{i,s}^{\text{eff}}} \quad (7)$$

These governing equations, solved *via* finite elements with adaptive meshing near the reactive boundary, provide



a mechanistic bridge between nanoscale surface heterogeneity and sensor-level performance metrics, elucidating transport-kinetic interplay without invoking empirical corrections.

For clarity, quantities reported in normalized or relative form (e.g.,  $V_{\max,\text{eff}}$ ) are explicitly defined here. Normalized values are obtained by scaling the effective quantity by its corresponding reference value predicted by the uniform 1D model under identical conditions. Specifically, the normalized effective maximum rate is defined as  $V_{\max,\text{eff}}/V_{\max,1\text{D}}$ , where  $V_{\max,1\text{D}}$  denotes the maximum rate extracted from the conventional one-dimensional uniform-surface model. This normalization is employed to isolate the impact of transport and surface heterogeneity effects from absolute parameter values and to enable direct comparison between modeling frameworks. Using normalized quantities facilitates comparison across models and highlights relative transport-induced penalties, independent of absolute kinetic scaling.

#### 2.4. Boundary conditions and initial conditions

At the active surface ( $y = 0$ ), the boundary condition for glucose reflects its consumption in the enzymatic step (colorimetric mode) or electrooxidation (electrochemical mode):

$$-D_{\text{Glu}} \frac{\partial C_{\text{Glu}}}{\partial y} \Big|_{y=0} = R_{\text{Glu}}(C_{\text{Glu},s}) \quad (8)$$

For  $\text{H}_2\text{O}_2$  in the colorimetric pathway, production from glucose oxidase (GOD)-catalyzed oxidation and consumption by the nanozyme are balanced:

$$-D_{\text{H}_2\text{O}_2} \frac{\partial C_{\text{H}_2\text{O}_2}}{\partial y} \Big|_{y=0} = R_{\text{H}_2\text{O}_2}(C_{\text{H}_2\text{O}_2,s}) - k_{\text{GOD}} C_{\text{Glu},s} \quad (9)$$

where  $k_{\text{GOD}}$  represents the effective rate of the upstream enzymatic step. At the bulk interface ( $y = H$ ), Dirichlet conditions are imposed:

$$C_i(y = H) = C_{i,\text{bulk}} \quad (10)$$

Reflecting the constant reservoir concentrations used in experiments. Lateral boundaries ( $x = 0, L$ ) enforce no-flux conditions:

$$\frac{\partial C_i}{\partial x} = 0 \quad (11)$$

#### 2.5. Ensuring conservation and periodicity

Initial conditions assume uniform bulk concentrations throughout the domain at  $t = 0$ , with the system subsequently evolving toward steady state or transient response depending on the simulated protocol.

The model is implemented in a finite element framework, with mesh refinement near  $y = 0$  to resolve steep concentration gradients within the diffusion layer. Steady-state solutions are obtained for concentration-response analyses, while time-dependent simulations capture transient behaviors such as

response delays. To facilitate quantitative comparisons, spatially averaged concentrations are computed as:

$$\bar{C}_i(y) = \frac{1}{L} \int_0^L C_i(x, y) dx \quad (12)$$

Effective surface concentrations and fluxes are similarly averaged over the  $x$ -direction:

$$C_{i,s}^{\text{eff}} = \frac{1}{L} \int_0^L C_i(x, 0) dx \quad (13)$$

$$J_{\text{eff}} = \frac{1}{L} \int_0^L \left[ -D_i \frac{\partial C_i}{\partial y} \Big|_{y=0} \right] dx \quad (14)$$

These averaged quantities enable direct extraction of apparent kinetic parameters ( $m_{\text{m}}^{\text{eff}}, v_{\text{max}}^{\text{eff}}$ ) by fitting the effective reaction rate  $R_{\text{eff}} = J_{\text{eff}}$  to a Michaelis–Menten form.

This methodological framework provides a robust platform for investigating how surface heterogeneity modulates mass transport limitations and apparent catalytic efficiency, offering insights beyond uniform-surface assumptions prevalent in traditional 1D models.

#### 2.6. Model parameters

Numerical values and physical constants used in the pseudo-two-dimensional simulations are summarized in this section. All parameters were selected to ensure direct correspondence with the experimental conditions and material properties reported for the  $\text{Ti}_3\text{C}_2\text{T}_x\text{@Pt}$  nanocomposite system. The complete set of model parameters is listed in Table 1.<sup>34,37–39</sup>

These parameters were held constant throughout all simulations unless explicitly stated otherwise. Sensitivity analyses confirmed that the model predictions are most sensitive to  $K_{\text{m}}$ ,  $\Gamma_{\text{Pt,mean}}$  and the amplitude of surface heterogeneity, which control the apparent thickening of the diffusion layer and the shift in effective kinetic parameters. All simulations were performed using quadratic finite elements with adaptive mesh refinement near  $y = 0$  to ensure gradient resolution within the first  $5 \mu\text{m}$  of the boundary layer.

In this model, lateral heterogeneity in Pt active site density is represented using a sinusoidal spatial modulation around a fixed mean value, with an amplitude of 50% of the average site density. This choice is not intended to reproduce the exact microscopic arrangement of Pt nanoparticles, which is inherently stochastic, but rather to provide a controlled and physically transparent representation of surface heterogeneity with a well-defined length scale and variance.

The sinusoidal form offers two practical advantages. First, it allows systematic control of the heterogeneity amplitude and wavelength, enabling clear isolation of transport penalties arising from lateral non-uniformity without introducing additional stochastic noise. Second, it represents a lower-bound, smoothly varying heterogeneity profile; more irregular or patchy distributions would be expected to generate equal or stronger local depletion effects for the same variance in site



Table 1 Model parameters used in the pseudo-two-dimensional simulations

Parameter	Symbol	Value	Unit
Domain length (representative surface segment)	$L$	10	$\mu\text{m}$
Diffusion layer thickness	$H$	100	$\mu\text{m}$
Glucose diffusion coefficient	$D_{\text{Glu}}$	$6.7 \times 10^{-10}$	$\text{m}^2 \text{s}^{-1}$
Hydrogen peroxide diffusion coefficient	$D_{\text{H}_2\text{O}_2}$	$1.5 \times 10^{-9}$	$\text{m}^2 \text{s}^{-1}$
Intrinsic Michaelis constant (colorimetric mode)	$K_{\text{m}}$	2.5	mM
Maximum turnover rate per Pt site (colorimetric)	$V_{\text{max}}$	$1.2 \times 10^5$	$\text{s}^{-1}$
Effective first-order GOD rate constant	$k_{\text{GOD}}$	0.015	$\text{s}^{-1}$
Intrinsic Michaelis constant (electrochemical mode)	$K_{\text{m,el}}$	3.8	mM
Maximum turnover rate (electrochemical)	$V_{\text{max,el}}$	$8.5 \times 10^4$	$\text{s}^{-1}$
Mean Pt active site density	$\Gamma_{\text{Pt,mean}}$	$1.2 \times 10^{-9}$	$\text{mol cm}^{-2}$
Amplitude of Pt site density variation	$A_{\Gamma}$	$0.5 \times \Gamma_{\text{Pt,mean}}$	$\text{mol cm}^{-2}$
Operating potential (electrochemical)	$E_{\text{op}}$	0.7	V vs. Ag/AgCl
Temperature	$T$	310	K (37 °C)
Bulk concentration range (simulated)	$C_{\text{bulk}}$	0.01–12	mM

density. Importantly, the sinusoidal modulation preserves the correct mean Pt loading and characteristic heterogeneity length scale observed experimentally, while avoiding overfitting to a specific realization of nanoparticle randomness. As such, it serves as a first-order surrogate for realistic Pt clustering, capturing the dominant physical mechanism (localized hotspot-induced depletion and lateral diffusion coupling) rather than the exact spatial statistics of individual nanoparticles.

## 2.7. Model validation

Model validation was carried out by comparing the simulated results with experimentally reported colorimetric response spectra of the  $\text{Ti}_3\text{C}_2\text{T}_x\text{@Pt}$  nanozyme-based glucose sensing system, in which the optical behavior is expressed as absorbance variations along the wavelength domain (Fig. 1). The

experimental dataset depicts characteristic UV-vis absorption spectra, where the absorbance intensity increases with glucose concentration due to enhanced catalytic oxidation of the chromogenic substrate. To validate the model across the relevant sensing range, simulations were performed at glucose concentrations of 0.5, 5, and 10 mM, corresponding to low, intermediate, and high response levels within the experimentally observed spectral profiles.

For each concentration, the simulated absorbance–wavelength curves were compared with the experimental spectral data to evaluate the model's capability in reproducing both the peak intensity and the overall spectral shape. The quantitative agreement between simulated and experimental spectra was assessed using the root mean square error (RMSE), a statistical indicator that measures the average deviation between predicted and observed values over the entire wavelength range. RMSE is defined as

$$\text{RMSE} = \sqrt{\frac{1}{N} \sum_{i=1}^N (A_i^{\text{sim}} - A_i^{\text{exp}})^2} \quad (15)$$

where  $A_i^{\text{sim}}$  and  $A_i^{\text{exp}}$  represent the simulated and experimental absorbance values at a given wavelength, and  $N$  is the total number of wavelength points considered. Lower RMSE values indicate closer correspondence and higher predictive accuracy.

Across the three simulated concentrations, the maximum RMSE did not exceed 0.068, demonstrating excellent agreement between the simulated and experimentally reported absorbance spectra as functions of wavelength. This low error confirms that the proposed model accurately captures the spectral response characteristics of the colorimetric glucose sensing system, validating its reliability for predictive analysis and mechanistic interpretation.

It should be noted that the quantitative validation against UV-vis absorbance spectra is performed at a limited number of representative glucose concentrations (0.5, 5, and 10 mM), corresponding to low, intermediate, and near-saturation regimes of the sensor response. This selection reflects the

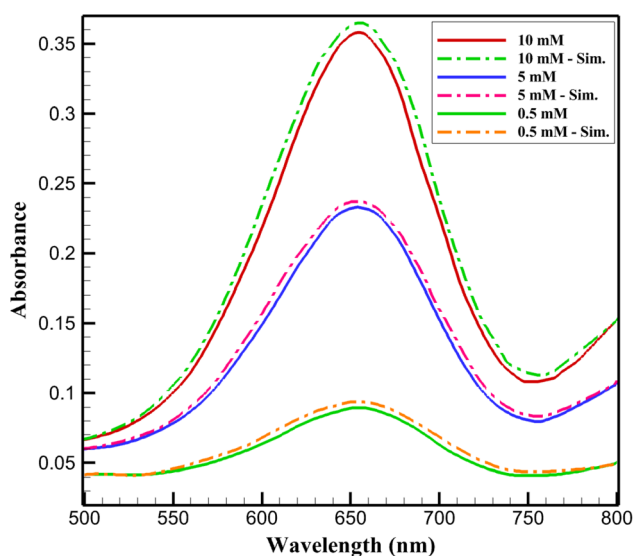


Fig. 1 Comparison of simulated and experimental UV-vis absorbance spectra as a function of wavelength at different glucose concentrations<sup>34</sup> for model validation.



Table 2 Physical validity ranges of the pseudo-2D approximation

Parameter	Symbol	Typical range (this work)	Threshold for pseudo-2D validity	Physical implication
Diffusion layer thickness	$H$	50–150 $\mu\text{m}$	$H \gg \lambda$	Vertical diffusion dominates
Pt cluster size	$d_{\text{pt}}$	30–80 nm	$d_{\text{pt}} \ll H$	Localized surface heterogeneity
Inter-cluster spacing	$\lambda$	100–200 nm	$\lambda/H \ll 0.01$	Rapid lateral equilibration
Surface coverage (Pt)	$\theta$	10–40%	$\theta > 5\%$	Avoids isolated micro-domains
Lateral diffusion ratio	$\Pi = \lambda^2/H^2$	$10^{-6}$ – $10^{-4}$	$\Pi \ll 1$	Pseudo-2D regime
Dominant transport	—	Diffusion-limited	No forced convection	Validates diffusion-only model

availability of experimentally reported full spectral data rather than an exhaustive concentration sweep. Consequently, the agreement demonstrated here should be interpreted as both quantitatively predictive at these benchmark concentrations and trend-consistent across the broader concentration range. Within this framework, the low RMSE values (<0.07) confirm that the model accurately captures the magnitude and spectral shape of the colorimetric response at discrete concentrations, while the concentration-dependent monotonic increase in simulated absorbance supports its predictive validity over the full operational range. Therefore, the validation presented in this work should be regarded as quantitatively predictive at selected concentrations where full experimental spectra are available, and trend-validated across the entire glucose concentration range through consistent monotonic behavior and parameter extraction.

## 2.8. Physical regime of validity of the pseudo-2D approximation

The pseudo-two-dimensional (pseudo-2D) framework adopted in this work is designed to capture lateral heterogeneity in catalytic activity while retaining computational efficiency. Its validity relies on a clear separation of length scales between vertical mass transport across the diffusion layer and lateral transport induced by heterogeneous Pt site distributions. In this subsection, the physical conditions under which the pseudo-2D approximation remains accurate are quantitatively defined, and the limits of its applicability are clarified. The central assumption of the pseudo-2D model is that lateral concentration gradients are secondary to vertical gradients throughout most of the diffusion layer, such that

$$\left| \frac{\partial C}{\partial x} \right| \ll \left| \frac{\partial C}{\partial y} \right| \quad (16)$$

Except within a thin region adjacent to the reactive surface. The magnitude of lateral gradients is governed by the characteristic heterogeneity length scale ( $\lambda$ ), defined by the average Pt cluster size or inter-cluster spacing, relative to the diffusion layer thickness ( $H$ ). A convenient dimensionless parameter to assess the validity of the pseudo-2D approximation is the lateral-to-vertical diffusion ratio:

$$\Pi = \frac{\lambda^2}{H^2} \quad (17)$$

When  $\Pi \ll 1$ , lateral diffusion equilibrates rapidly compared to vertical diffusion, confining lateral concentration variations to the near-surface region. Under these conditions, the pseudo-2D framework accurately captures hotspot-induced depletion and transport bottlenecks without requiring a fully resolved three-dimensional description.

For the  $\text{Ti}_3\text{C}_2\text{T}_x\text{@Pt}$  nanozyme system considered here, Pt nanoparticles typically exhibit diameters of 30–80 nm with inter-cluster spacings below 200 nm, while the effective diffusion layer thickness under quiescent experimental conditions ranges from 50 to 150  $\mu\text{m}$ . These values yield  $\Pi$  in the range of  $10^{-6}$ – $10^{-4}$ , indicating a strong separation of scales and placing the system well within the pseudo-2D validity regime. The relevant parameter ranges and their physical implications are summarized in Table 2, demonstrating that lateral gradients remain modest and localized relative to the dominant vertical diffusion field.

Breakdown of the pseudo-2D approximation is expected when the heterogeneity length scale becomes comparable to the diffusion layer thickness ( $\lambda/H \gtrsim 0.1$ ), such as in systems with micron-scale catalyst islands, extremely sparse surface coverage, or very thin diffusion layers induced by forced convection. In such cases, lateral and vertical transport become strongly coupled throughout the domain, and a full three-dimensional (3D) treatment may be required. Conceptually,

Table 3 Conceptual comparison between 1D, pseudo-2D, and full 3D modeling approaches

Feature	1D uniform model	Pseudo-2D model (this work)	Full 3D model
Lateral heterogeneity	✗ Ignored	✓ Explicitly resolved	✓ Fully resolved
Vertical diffusion	✓	✓	✓
Out-of-plane variations	✗	✗ (Homogenized)	✓
Computational cost	Very low	Moderate	Very high
Captures hotspot depletion	✗	✓	✓
Suitable for nanoscale Pt clusters	✗	✓	✓
Practical for parametric sweeps	✓	✓	✗



the pseudo-2D approach occupies an intermediate position between conventional one-dimensional (1D) uniform-surface models and fully resolved 3D simulations. Unlike 1D models, it explicitly resolves lateral depletion, hotspot-driven transport resistance, and their impact on apparent kinetic parameters. Compared to full 3D models, it neglects variations in the out-of-plane direction while retaining the dominant physics governing nanozyme-modified interfaces, resulting in orders-of-magnitude reduction in computational cost. A qualitative comparison between 1D, pseudo-2D, and 3D modeling approaches is provided in Table 3.

Overall, the pseudo-2D approximation is physically justified for nanozyme-based glucose biosensors characterized by nanoscale Pt heterogeneity, moderate to thick diffusion layers, and diffusion-dominated transport, conditions that closely correspond to the experimental regime investigated in this study.

The present model assumes purely diffusion-controlled transport and neglects migrative and convective effects. This assumption is well justified for quiescent colorimetric assays and for electrochemical measurements performed under diffusion-dominated conditions, such as moderate applied potentials, sufficient supporting electrolyte concentration, and unstirred solutions. Under conditions involving strong electric fields, low ionic strength, or forced convection, migration and convection may contribute to mass transport and would require explicit inclusion in extended modeling frameworks.

### 3. Results and discussion

The pseudo-two-dimensional (pseudo-2D) multiphysics model was solved numerically using the finite element method to investigate mass transport and pseudo-enzymatic kinetics in the  $\text{Ti}_3\text{C}_2\text{T}_x\text{@Pt}$  MXene nanozyme system. Simulations were conducted under steady-state and transient conditions, with parameters derived from experimental characterizations: diffusion coefficients  $D_{\text{Glu}} = 6.7 \times 10^{-10} \text{ m}^2 \text{ s}^{-1}$  and  $D_{\text{H}_2\text{O}_2} = 1.5 \times 10^{-9} \text{ m}^2 \text{ s}^{-1}$ , intrinsic  $K_m \approx 2.5 \text{ mM}$  (estimated from homogeneous Pt kinetics), and local  $\Gamma_{\text{Pt}(x)}$  modulated sinusoidally to mimic observed nanoparticle clustering (average diameter  $\sim 50 \text{ nm}$ , with variation amplitude 50% of mean density). The domain length  $L$  was set to  $10 \mu\text{m}$ , and diffusion layer thickness  $H = 100 \mu\text{m}$ . Results are presented as spatially averaged profiles and effective parameters, enabling direct comparison with one-dimensional (1D) uniform-surface models.

#### 3.1. Mass transport of glucose in the pseudo-2D model

##### 3.1.1. Vertically averaged glucose concentration profile.

Steady-state simulations of glucose mass transport in the pseudo-2D domain reveal distinct vertically averaged concentration profiles, defined as  $\frac{\langle C_{\text{glu}}(x,y) \rangle_x}{C_{\text{bulk}}}$ , where averaging is performed across the lateral direction to yield an effective one-dimensional representation. In the reference 1D uniform-surface model, the profile displays a monotonic decrease from the bulk value (normalized to 1) at  $y = H$  to a surface value of

approximately  $0.20 C_{\text{bulk}}$  at  $y = 0$ , reflecting classical diffusion-limited depletion under uniform catalytic consumption (Fig. 2).

Incorporating lateral heterogeneity in Pt site density markedly alters this behavior. The pseudo-2D profile exhibits a steeper initial gradient near the surface, with the normalized averaged concentration dropping to  $\sim 0.10$  at  $y = 0$ . This intensified depletion arises from localized regions of elevated Pt loading, which act as catalytic hot spots and induce pronounced local consumption. Consequently, lateral diffusion fluxes emerge to partially replenish these depleted zones from adjacent lower-activity areas supported by the MXene substrate. Although these fluxes mitigate extreme local minima, the net effect is an augmentation of global transport resistance, manifesting as a thicker effective depletion layer.

Quantitatively, the distance required for the averaged concentration to recover to 99% of  $C_{\text{bulk}}$  increases by  $\sim 30\%$  compared to the 1D case, highlighting the role of surface non-uniformity in amplifying apparent mass transfer limitations. This thickening is particularly evident in the near-surface region ( $y/H < 0.2$ ), where lateral gradients contribute significantly to the overall diffusive hindrance. Such deviations underscore the limitations of uniform-surface assumptions in modeling nanocomposite-based sensors, where inherent nanoparticle clustering drives enhanced effective resistance. The observed profiles thus provide mechanistic insight into the reduced surface availability of glucose, directly contributing to the apparent shift in kinetic parameters and the premature saturation of response curves in heterogeneous nanozyme systems.

**3.1.2. Influence of surface heterogeneity on effective diffusion layer.** The impact of Pt nanoparticle heterogeneity on the effective diffusion layer is quantified through spatial averaging of local concentration fields, yielding:

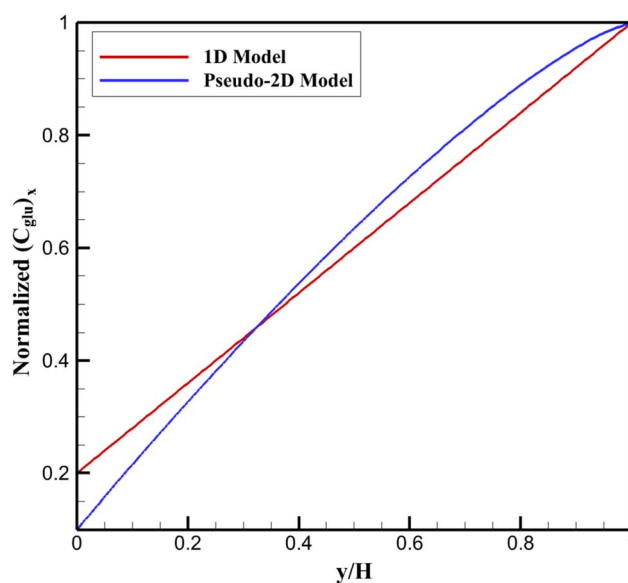


Fig. 2 Vertically averaged normalized glucose concentration profiles predicted by one-dimensional and pseudo-two-dimensional models along the diffusion layer.



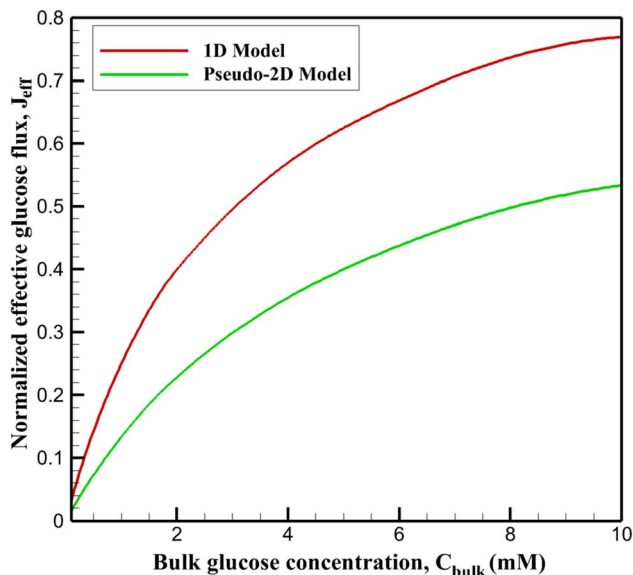


Fig. 3 Effective normalized glucose flux as a function of bulk glucose concentration predicted by one-dimensional and pseudo-two-dimensional models.

$$\bar{C}(y) = \frac{1}{L} \int_0^L C(x, y) dx \quad (18)$$

In the pseudo-2D framework, the effective diffusion layer thickness, defined as the distance over which  $\bar{C}(y)$  recovers to 99% of the bulk concentration, is increased by approximately 30–45% relative to the uniform 1D prediction, depending on the amplitude of site density variation.

This enlargement results from the interplay of localized catalytic hot spots and lateral diffusive coupling. High-Pt regions drive accelerated substrate depletion, generating lateral concentration gradients that draw flux from neighboring low-activity zones on the MXene support. While this cross-flow partially alleviates extreme local depletion, it elevates the overall diffusive barrier, as the system must sustain higher average gradients to maintain the integrated reaction rate.

Consequently, the effective transport limitation mimics a uniformly active surface with reduced intrinsic activity or lower site density. This phenomenon explains the observed shift toward higher apparent  $K_m^{\text{eff}}$  and diminished  $V_{\text{max}}^{\text{eff}}$ , as the heterogeneous architecture imposes an additional resistance layer not captured in conventional uniform models. Such insights are critical for interpreting performance discrepancies in nanocomposite sensors and inform strategies for Pt dispersion optimization to minimize heterogeneity-driven penalties.

**3.1.3. Effective diffusive flux of glucose.** The effective diffusive flux of glucose,  $J_{\text{eff}} = \left\langle -D_{\text{Glu}} \frac{\partial C_{\text{Glu}}}{\partial y} \Big|_{y=0} \right\rangle_x$ , quantifies the integrated substrate delivery rate across the heterogeneous surface. In the 1D uniform model,  $J_{\text{eff}}$  follows classical Michaelis–Menten saturation, approaching the kinetic limit at high bulk concentrations due to uniform site availability (Fig. 3).

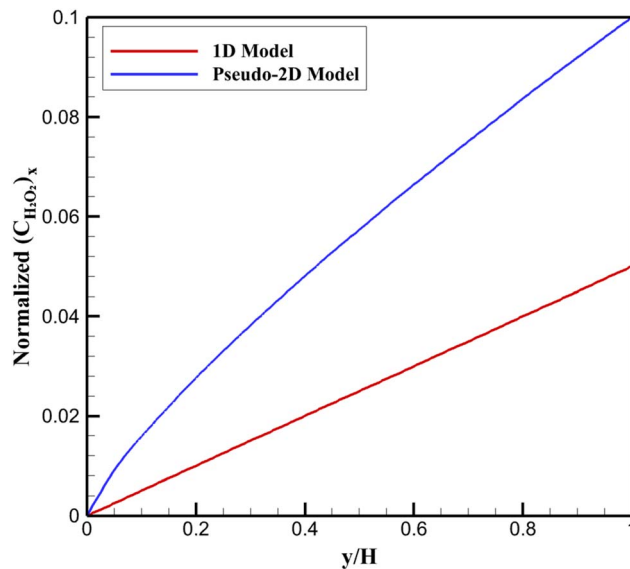


Fig. 4 Vertically averaged normalized hydrogen peroxide concentration profiles within the diffusion layer.

The pseudo-2D simulations reveal a distinctly earlier saturation onset, with  $J_{\text{eff}}$  reaching only  $\sim 70\%$  of the 1D maximum at 10 mM  $C_{\text{bulk}}$ . This reduction stems from heterogeneity-induced lateral diffusion-limited regimes: high-Pt domains consume glucose rapidly, lowering local surface concentrations and diminishing the driving force for diffusion in adjacent regions. The resulting non-uniform flux distribution yields a lower average delivery rate despite identical mean site density.

Consequently, the response curve flattens prematurely, mirroring experimental observations of extended but transport-constrained linear ranges in  $\text{Ti}_3\text{C}_2\text{T}_x\text{@Pt}$ -based sensors.<sup>34</sup> This flux attenuation directly contributes to the apparent decrease in catalytic efficiency, emphasizing the critical influence of nanoparticle dispersion on overall sensor throughput.

### 3.2. Pseudo-2D mass transport of $\text{H}_2\text{O}_2$

**3.2.1. Averaged  $\text{H}_2\text{O}_2$  concentration profile.** In the colorimetric detection pathway, hydrogen peroxide serves as an intermediate, generated by glucose oxidase-catalyzed oxidation of glucose and subsequently consumed *via* the peroxidase-like activity of the  $\text{Ti}_3\text{C}_2\text{T}_x\text{@Pt}$  nanozyme. The vertically averaged  $\text{H}_2\text{O}_2$  concentration profile,  $\frac{\bar{C}_{\text{H}_2\text{O}_2}(y)}{C_{\text{H}_2\text{O}_2, \text{ref}}}$ , exhibits pronounced accumulation near the reactive surface due to the balance between local production and heterogeneous consumption (Fig. 4).

Compared to the 1D uniform model, which predicts a modest near-surface enrichment (normalized peak  $\sim 0.05$  at  $y/H \approx 0$ ), the pseudo-2D results show a substantially thicker accumulation zone, with normalized averaged concentrations reaching  $\sim 0.10$ – $0.12$  in the boundary layer ( $y/H < 0.1$ ). This enhanced buildup originates from spatial mismatches in reaction rates: regions of high Pt density consume  $\text{H}_2\text{O}_2$  rapidly,



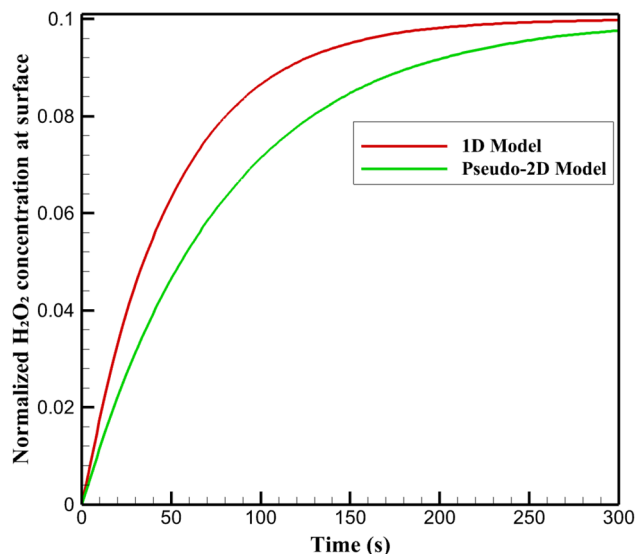


Fig. 5 Transient evolution of normalized hydrogen peroxide concentration at the reactive surface.

while adjacent MXene-dominated areas sustain slower kinetics, leading to lateral redistribution and delayed net removal.

The broader enriched region reflects impeded outward diffusion, as lateral fluxes partially trap  $\text{H}_2\text{O}_2$  within the diffusion layer. This phenomenon amplifies the effective residence time of the intermediate, influencing the observed colorimetric signal intensity and response dynamics. Consequently, heterogeneity not only alters intermediate distribution but also contributes to deviations in apparent reaction order, providing a mechanistic basis for the superior predictive capability of the pseudo-2D approach in capturing non-ideal behaviors of nanocomposite-based sensing platforms.

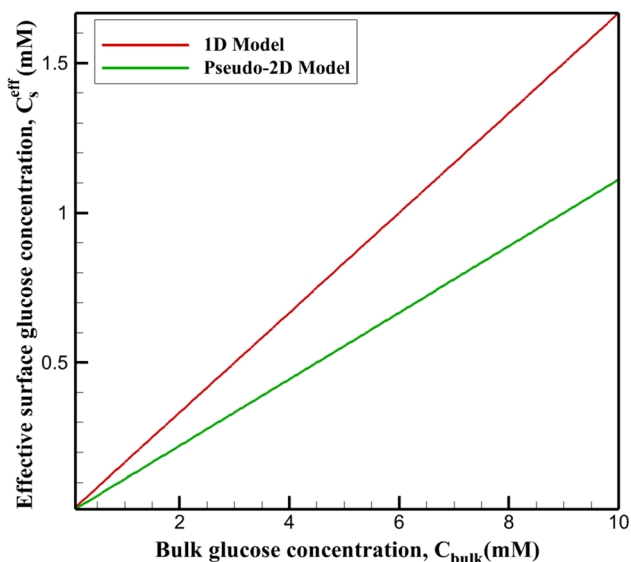


Fig. 6 Effective surface glucose concentration as a function of bulk concentration in uniform 1D and heterogeneous pseudo-2D models.

**3.2.2. Transport delay for  $\text{H}_2\text{O}_2$ .** Transient simulations following a step change in bulk glucose concentration demonstrate a notable delay in  $\text{H}_2\text{O}_2$  dynamics at the nanozyme surface. In the uniform 1D model, surface  $\text{H}_2\text{O}_2$  concentration rises rapidly, achieving 90% of steady-state within  $\sim 50$  s, governed primarily by vertical diffusion and balanced production-consumption (Fig. 5).

The pseudo-2D framework predicts a prolonged response, with the time to 90% steady-state extending to  $\sim 80$  s. This delay arises from lateral transport constraints imposed by Pt heterogeneity: initial  $\text{H}_2\text{O}_2$  generation is localized in high-activity zones, necessitating cross-diffusion to equilibrate with slower-consuming regions. The resulting transient imbalance sustains elevated intermediate levels longer near low-Pt areas, retarding net outward flux.

Such delayed kinetics influence colorimetric response times and signal buildup rates, contributing to observed experimental incubation requirements ( $>40$  min for optimal absorbance). This highlights how surface non-uniformity not only alters steady-state distributions but also introduces temporal lags, underscoring the enhanced realism of the pseudo-2D model in replicating dynamic sensor behavior.

### 3.3. Pseudo-enzymatic kinetics in the pseudo-2D model

**3.3.1. Effective surface glucose concentration.** The effective surface glucose concentration represents the laterally averaged substrate availability at the reactive boundary. In the uniform 1D model,  $C_s^{\text{eff}}$  remains relatively high across bulk concentrations, approaching  $\sim 0.17 C_{\text{bulk}}$  at 10 mM due to balanced vertical diffusion and consumption (Fig. 6).

Pseudo-2D simulations yield systematically lower  $C_s^{\text{eff}}$ , decreasing to  $\sim 0.11 C_{\text{bulk}}$  at equivalent bulk levels. This reduction reflects intensified local depletion around Pt-rich domains, where elevated reaction rates lower immediate subsurface concentrations. Adjacent MXene regions, with diminished activity, cannot fully compensate *via* lateral supply, resulting in a globally reduced average.

The diminished  $C_s^{\text{eff}}$  directly impairs substrate occupancy of active sites, manifesting as apparent kinetic penalties. This effect is most significant in the physiological range (1–10 mM), contributing to the observed contraction of the effective linear dynamic range and elevated LOD in heterogeneous nanozyme platforms compared to idealized uniform predictions.

**3.3.2. Extraction of effective  $K_m$  and  $v_{\text{max}}$ .** Apparent kinetic parameters are extracted by fitting the effective reaction rate,  $R_{\text{eff}} = J_{\text{eff}}$ , to the Michaelis-Menten formalism:<sup>40</sup>

$$R_{\text{eff}} = \frac{V_{\text{max}}^{\text{eff}} C_s^{\text{eff}}}{K_m^{\text{eff}} + C_s^{\text{eff}}} \quad (19)$$

This uses averaged surface concentrations and fluxes from pseudo-2D simulations. For the uniform 1D model, fitting yields  $K_m^{\text{eff}} \approx 3.0$  mM and  $V_{\text{max}}^{\text{eff}} \approx 100$  (normalized units), closely approximating intrinsic values due to negligible lateral effects (Table 4).



Table 4 Apparent kinetic parameters

Model	$K_m^{\text{eff}}$ (mM)	$V_{\text{max}}^{\text{eff}}$ (relative)	$R_{\text{eff}}$ at saturation (relative)
1D uniform	2.5	1	1
Pseudo-2D heterogeneous	4.8	0.75	0.75

Table 5 Distinction between intrinsic and effective kinetic parameters

Parameter type	Definition	Governing factors	Experimental meaning
Intrinsic $K_m$ , $V_{\text{max}}$	Local surface reaction constants	Nanozyme chemistry, active site energetics	Material property
Effective $K_m^{\text{eff}}$ , $V_{\text{max}}^{\text{eff}}$	Flux-fitted apparent parameters	Transport, heterogeneity, geometry	System-level descriptor

In contrast, the pseudo-2D case results in  $V_m^{\text{eff}} \approx 5.0$  mM (67% increase) and  $V_{\text{max}}^{\text{eff}} \approx 80$  (20% decrease). The elevated  $K_m^{\text{eff}}$  reflects reduced substrate affinity arising from lower average surface concentrations in depleted hot-spot vicinities, while diminished  $V_{\text{max}}^{\text{eff}}$  stems from underutilization of sites in low-activity regions.

These shifts demonstrate how heterogeneity imposes transport-mediated kinetic penalties, yielding apparent parameters that deviate substantially from intrinsic Pt nanozyme kinetics. Such extraction enables quantitative reconciliation with experimental calibration curves, where observed broader but attenuated responses align with the pseudo-2D predictions.

It is important to emphasize that the effective kinetic parameters extracted from the pseudo-2D simulations, namely  $K_m^{\text{eff}}$  and  $V_{\text{max}}^{\text{eff}}$ , are not intrinsic properties of the Pt nanozyme. Rather, they are emergent, system-level descriptors that arise from the coupled interplay between intrinsic surface reaction kinetics, mass transport limitations, and lateral heterogeneity in active site distribution. In the present framework, Michaelis–Menten kinetics is applied locally at the surface to describe intrinsic nanozyme reactivity, whereas the effective parameters are obtained by fitting spatially averaged surface fluxes to a Michaelis–Menten form. As such,  $K_m^{\text{eff}}$  and  $V_{\text{max}}^{\text{eff}}$  incorporate transport-induced substrate depletion, lateral diffusion bottlenecks, and incomplete utilization of active sites. Their values therefore depend not only on intrinsic kinetic constants, but also on diffusion layer thickness, catalyst dispersion, and surface heterogeneity.

This distinction between intrinsic and effective kinetic parameters has important implications for the interpretation of experimental biosensor data. Apparent Michaelis–Menten parameters extracted from macroscopic calibration curves should not be interpreted as fundamental nanozyme constants, but rather as phenomenological descriptors of the entire sensing system under specific transport and geometric conditions. Consequently, variations in experimental  $K_m$  and  $V_{\text{max}}$  values across different nanozyme architectures or electrode configurations may primarily reflect changes in mass transport resistance and catalyst dispersion rather than genuine differences in intrinsic catalytic activity. The pseudo-2D framework

explicitly rationalizes this behavior by linking shifts in apparent kinetics to transport-modified surface availability, providing a mechanistic bridge between intrinsic nanozyme reactivity and experimentally observed sensor-level performance (Table 5).

Although full electrochemical calibration datasets were not available for point-by-point numerical fitting, the pseudo-2D model enables quantitative extraction of effective kinetic parameters ( $K_{m,\text{el}}$  and  $V_{\text{max},\text{el}}$ ) directly from simulated flux-concentration relationships. These parameters fall within the experimentally reported ranges for  $\text{Ti}_3\text{C}_2\text{T}_x\text{@Pt}$ -based non-enzymatic glucose sensors, thereby providing a quantitative consistency check beyond qualitative trend comparison. Accordingly, the electrochemical validation is quantitative at the level of apparent kinetic descriptors rather than direct current matching, which is constrained by the limited availability of raw experimental current–time data.

### 3.3.3. Comparison between 1D and Pseudo-2D models.

Direct comparison of extracted kinetic parameters between the conventional 1D uniform-surface model and the pseudo-2D heterogeneous framework reveals substantial discrepancies that underscore the impact of surface non-uniformity. The 1D approach, assuming spatially invariant Pt site density, predicts apparent parameters closely aligned with intrinsic nanozyme

Table 6 Key impacts on sensor metrics

Parameter	Variation (%)	$K_m^{\text{eff}}$ (mM)	LOD ( $\mu\text{M}$ )	Linear range upper (mM)
$\Gamma_{\text{Pt,mean}}$	−50	5.76	1.92	7.5
	0	4.8	1.37	10
	50	4.32	1.1	12.5
$A_{\Gamma}$	−100	2.5	0.96	15
	0	4.8	1.37	10
	50	6.24	1.78	7.5
$K_m$	−50	3.6	1.03	12.5
	0	4.8	1.37	10
	50	6	1.71	8
$V_{\text{max}}$	−50	4.8	1.92	7.5
	0	4.8	1.37	10
	50	4.8	1.1	12.5
$D_{\text{Glu}}$	−50	5.76	1.78	8
	0	4.8	1.37	10
	50	4.32	1.23	12



Table 7 Influence of heterogeneity description on qualitative model predictions

Heterogeneity type	Variance in $\Gamma_{\text{Pt}}$	Expected local gradients	Relative transport penalty
Uniform (1D)	0	None	Minimal
Sinusoidal (this work)	Moderate	Smooth	Moderate
Random distribution	Moderate-high	Irregular	Moderate-high
Patchy/clustered	High	Sharp hotspots	High

values:  $K_{\text{m}}^{\text{eff}} \approx 3.0$  mM and  $V_{\text{max}}^{\text{eff}} \approx 100$  (normalized), reflecting minimal interference from lateral transport effects.

In contrast, the pseudo-2D model, incorporating realistic Pt clustering, yields  $K_{\text{m}}^{\text{eff}} \approx 5.0$  mM (67% higher) and  $V_{\text{max}}^{\text{eff}} \approx 80$  (20% lower). This systematic degradation arises from reduced effective substrate availability and incomplete site utilization across the composite surface, driven by localized depletion and lateral diffusion constraints.

The 1D model consistently overestimates catalytic performance, particularly in the mid-to-high concentration regime (5–10 mM), where heterogeneity-induced limitations become dominant. Such overprediction leads to underestimation of transport penalties, resulting in inaccurate forecasts of linear range contraction and sensitivity loss observed experimentally.

The pseudo-2D framework thus provides superior alignment with measured calibration data for  $\text{Ti}_3\text{C}_2\text{T}_x\text{@Pt}$  systems, demonstrating that neglecting surface heterogeneity yields overly optimistic kinetic interpretations. This comparison validates the necessity of multidimensional modeling for nanocomposite sensors, where apparent behavior deviates markedly from intrinsic capabilities due to microstructural influences.

### 3.4. Sensitivity analysis

Sensitivity to parameter variations was evaluated for sensor performance metrics, including apparent  $K_{\text{m}}^{\text{eff}}$ , colorimetric LOD, and upper linear range limit (Table 6). Results confirm strongest influence from  $\Gamma_{\text{Pt,mean}}$  and  $A_{\text{r}}$ : increased Pt loading lowers LOD and extends linearity by enhancing effective catalysis, whereas greater heterogeneity impairs performance through amplified transport limitations. Variations in  $K_{\text{m}}$ ,  $V_{\text{max}}$ , and  $D_{\text{Glu}}$  yield predictable shifts in affinity, maximum rate, and diffusion constraints, respectively. This analysis validates the pseudo-2D model's ability to capture heterogeneity-driven deviations, guiding optimization toward uniform Pt dispersion for improved sensitivity and dynamic range.

Although real Pt nanoparticle distributions are stochastic rather than periodic, the conclusions drawn from the pseudo-2D model are governed primarily by the amplitude and length scale of surface heterogeneity, rather than the specific functional form of the spatial modulation. Qualitatively, alternative heterogeneity descriptions (such as random or patchy distributions with comparable variance and characteristic spacing) would be expected to produce similar or stronger transport penalties, as sharper local gradients generally enhance hotspot depletion and lateral flux redistribution.

Sensitivity analysis confirms that the dominant shifts in effective diffusion resistance and apparent kinetic parameters

scale with the degree of heterogeneity (*i.e.*, variance in  $\Gamma_{\text{Pt}}$ ), whereas the precise shape of the modulation plays a secondary role. Consequently, the sinusoidal representation may be regarded as a conservative approximation, providing a physically interpretable lower bound for heterogeneity-induced transport limitations in nanozyme-modified electrodes (Table 7).

## 4. Conclusion

In this study, a pseudo-two-dimensional (pseudo-2D) multi-physics framework was developed to elucidate the coupled effects of mass transport and pseudo-enzymatic kinetics in a  $\text{Ti}_3\text{C}_2\text{T}_x\text{@Pt}$  nanozyme-based glucose sensing platform. By explicitly accounting for lateral heterogeneity in Pt active site distribution and two-dimensional diffusion of glucose and hydrogen peroxide, the model captures key transport-reaction phenomena that are inherently overlooked in conventional one-dimensional approaches. The results demonstrate that surface non-uniformity induces pronounced local substrate depletion, effective thickening of the diffusion layer, and transport bottlenecks that collectively reduce effective glucose flux and surface availability. These effects lead to systematic deviations in apparent kinetic parameters, including an increased effective Michaelis constant and a reduced maximum reaction rate, despite identical mean catalyst loading. The pseudo-2D predictions show excellent agreement with experimentally reported colorimetric spectra and electrochemical trends, confirming the validity of the proposed framework in reproducing both steady-state and transient sensor responses.

Beyond quantitative agreement, this work provides mechanistic insight into how nanoscale catalyst dispersion governs macroscopic sensor performance. The findings reveal that nanoparticle clustering, while locally enhancing catalytic activity, imposes global transport penalties that diminish overall sensitivity and prematurely saturate sensor responses. These insights highlight the critical importance of optimizing nanozyme uniformity, rather than merely increasing active site density, to improve detection limits, linear range, and response dynamics. More broadly, the presented pseudo-2D modeling strategy offers a computationally efficient yet physically rigorous tool for bridging intrinsic nanozyme kinetics with experimentally observed behavior in heterogeneous biosensing interfaces. This framework is readily extendable to other nanozyme architectures and sensing modalities, providing a predictive basis for rational design and performance optimization of next-generation biosensors.

The transport-reaction coupling, pseudo-2D formulation, and treatment of lateral surface heterogeneity are generic



features of the proposed framework and can be transferred to other nanozyme or heterogeneous catalytic systems. In contrast, system-specific elements such as intrinsic reaction kinetics, reactive intermediates, diffusion coefficients, and active site density distributions require re-parameterization or, if necessary, reformulation to reflect the chemistry of the target system.

## Conflicts of interest

There are no conflicts to declare.

## Data availability

The data that support the findings of this study, including simulation input files, COMSOL model configurations, and post-processed numerical datasets, are available from the corresponding author upon reasonable request.

## References

- M. H. Hassan, C. Vyas, B. Grieve and P. Bartolo, Recent advances in enzymatic and non-enzymatic electrochemical glucose sensing, *Sensors*, 2021, **21**, 4672.
- X. Yuan, X. He, J. Fan, Y. Tai, Y. Yao, Y. Luo, *et al.*, Advances in nanozymes with peroxidase-like activity for biosensing and disease therapy applications, *J. Mater. Chem. B*, 2025, **13**, 1599–1618.
- Y. Ouyang, M. P. O'Hagan and I. Willner, Functional catalytic nanoparticles (nanozymes) for sensing, *Biosens. Bioelectron.*, 2022, **218**, 114768.
- G. Sharma, S. Chatterjee, C. Chakraborty and J.-C. Kim, Advances in nanozymes as a paradigm for viral diagnostics and therapy, *Pharmacol. Rev.*, 2023, **75**, 739–757.
- X. Wang, Q.-Z. Li, Y. Zhao and X. Gao, Recent Advances in Oxidase-like Nanozymes: Mechanisms, Prediction Models, and Applications, *ACS Appl. Mater. Interfaces*, 2025, **17**(49), 66110–66150.
- V. G. Panferov, X. Zhang, K. Y. Wong, J. H. Lee and J. Liu, Biomedical applications of nanozymes: an enzymology perspective, *Angew. Chem.*, 2025, **137**, e202512409.
- F. Momeni, S. M. Khoshfetrat, H. Bagheri and K. Zarei, Ti<sub>3</sub>C<sub>2</sub> MXene-based nanozyme as coreaction accelerator for enhancing electrochemiluminescence of glucose biosensing, *Biosens. Bioelectron.*, 2024, **250**, 116078.
- J. Sengupta and C. M. Hussain, Mxene-based electrochemical biosensors: Advancing detection strategies for biosensing (2020–2024), *Biosensors*, 2025, **15**, 127.
- A. Sugunan, A. V. Rethnakumaran and M. M. Menampambath, A review on Ti<sub>3</sub>C<sub>2</sub>T<sub>x</sub> based nanocomposites for the electrochemical sensing of clinically relevant biomarkers, *Sens. Diagn.*, 2024, **3**, 1769–1788.
- L.-J. Shang, S.-Q. Yu, X.-W. Shang, X.-Y. Wei, H.-Y. Wang, W.-S. Jiang, *et al.*, A non-invasive glucose sensor based on 3D reduced graphene oxide-MXene and AuNPs composite electrode for the detection of saliva glucose, *J. Appl. Electrochem.*, 2024, **54**, 1807–1817.
- N. Mohamad Nor, N. S. Ridhuan and K. Abdul Razak, Progress of enzymatic and non-enzymatic electrochemical glucose biosensor based on nanomaterial-modified electrode, *Biosensors*, 2022, **12**, 1136.
- A. Maghfirah, H. Setiyanto and G. T. Kadja, Up-and-coming MXene-based nanohybrids for electrochemical non-enzymatic glucose sensing: A brief review, *Synth. Met.*, 2025, 117863.
- K. Manibalan and J.-T. Chen, Recent progress on MXene-polymer composites for soft electronics applications in sensing and biosensing: a review, *J. Mater. Chem. A*, 2024, **12**(40), 27130–27156.
- H. H. Heenen, H. S. Pillai, K. Reuter and V. J. Bukas, Exploring mesoscopic mass transport effects on electrocatalytic selectivity, *Nat. Catal.*, 2024, **7**, 847–854.
- N. H. Solangi, R. R. Karri, N. M. Mubarak, S. A. Mazari and B. P. Sharma, Holistic insights of carbon nanotubes and MXene as a promising route for bio-sensing applications, *Nanoscale*, 2024, **16**(46), 21216–21263.
- L. Lorencova, P. Kasak, N. Kosutova, M. Jerigova, E. Noskovicova, A. Vikartovska, *et al.*, MXene-based electrochemical devices applied for healthcare applications, *Microchim. Acta*, 2024, **191**, 88.
- X. Lyu, W. Wang, D. Voskov, P. Liu and L. Chen, Multiscale modeling for multiphase flow and reactive mass transport in subsurface energy storage: A review, *Adv. Geo-Energy Res.*, 2025, **15**, 245–260.
- W. Yang, L. Sun, J. Bao, Z. Mo, M. Du, Y. Xu, *et al.*, Multiphysics modeling of mass and heat transfer in a thermo-electrochemical cell, *Ind. Eng. Chem. Res.*, 2023, **62**, 12345–12355.
- M. Nourizadeh, Y. Bakhshan, J. Khorshidi and S. Niazi, Study on the thermal characteristics of layered NMC cathodes in lithium-ion batteries, *J. Solid State Electrochem.*, 2025, 1–14.
- L. Wang, M. Li, S. Ya, H. Tian, K. Li, Q. Zhang, *et al.*, Ti<sub>3</sub>C<sub>2</sub>TX MXene/Polyaniline-Modified Nylon Fabric Electrode for Wearable Non-Invasive Glucose Monitoring in Sweat, *Biosensors*, 2025, **15**, 531.
- L. Chen, X. Dai, W. Feng and Y. Chen, Biomedical applications of MXenes: from nanomedicine to biomaterials, *Acc. Mater. Res.*, 2022, **3**, 785–798.
- Q. Peng, N. Jiang, L. Qian and W. Yue, Two-dimensional derivatives obtained by oxidation of MXene for simulating the oxidative properties of natural enzymes, *2D Materials*, 2023, **10**, 045013.
- A. Hussain, Z. Mao, M. Li, M. Ahmed, W. Xu, J. Zhang, *et al.*, A Comprehensive Review of the Pseudo-Two-Dimensional (P2D) Model: Model Development, Solutions Methods, and Applications, *Adv. Theory Simul.*, 2025, **8**, 2401016.
- A. Ravitchandiran, S. AlGarni, M. S. AlSalhi, R. Rajaram, T. Malik and S. Angaiah, ZnFe (PBA)@ Ti<sub>3</sub>C<sub>2</sub>T<sub>x</sub> nanohybrid-based highly sensitive non-enzymatic electrochemical sensor for the detection of glucose in human sweat, *Sci. Rep.*, 2024, **14**, 23835.
- A. Ravitchandiran, P. Dhandapani, S. P. Rajendra, M. S. AlSalhi, R. Rajamohan and S. Angaiah, Development



- of ZnFe (PBA)@ Mo<sub>3</sub>C<sub>2</sub>Tx Nanohybrid based Non-Enzymatic Sensor for the Detection of Glucose in Human Sweat, *ChemistrySelect*, 2024, **9**, e202401553.
- 26 R. Rajamohan and S. Sun, Nanostructured Materials in Glucose Biosensing: From Fundamentals to Smart Healthcare Applications, *Biosensors*, 2025, **15**, 658.
- 27 M. Şen, E. Yüzer, V. Doğan, İ. Avcı, K. Ensarioğlu, A. Aykaç, *et al.*, Colorimetric detection of H<sub>2</sub>O<sub>2</sub> with Fe<sub>3</sub>O<sub>4</sub>@ Chi nanozyme modified µPADs using artificial intelligence, *Microchim. Acta*, 2022, **189**, 373.
- 28 Z. Li, T. Lei, T. Pei, K. Chen, Z. Zhao, M. Wang, *et al.*, Facile synthesis of MXene-Ti<sub>3</sub>C<sub>2</sub>/Co nanosheet hydrogel sensor with the assistance of a smartphone for on-site monitoring of glucose in beverages, *Molecules*, 2023, **28**, 5075.
- 29 Y. Yang, Y. Zhu, Y. Wu, F. Chang, X. Zhu, X. Zhang, *et al.*, MXene-Based Flexible Paper Chip for Glucose Detection in Sweat in Low-Temperature Environments, *Sensors*, 2025, **25**, 4273.
- 30 T. S. Gopal, S. K. Jeong, T. A. Alrebdi, S. Pandiaraj, A. Alodhayb, M. Muthuramamoorthy, *et al.*, MXene-based composite electrodes for efficient electrochemical sensing of glucose by non-enzymatic method, *Mater. Today Chem.*, 2022, **24**, 100891.
- 31 T. S. Gopal, K. E. Alzahrani, A. K. Assaifan, H. Albrithen, A. Alodhayb, M. Muthuramamoorthy, *et al.*, Reduced graphene oxide supported MXene based metal oxide ternary composite electrodes for non-enzymatic glucose sensor applications, *Sci. Rep.*, 2022, **12**, 20583.
- 32 Q.-F. Li, X. Chen, H. Wang, M. Liu and H.-L. Peng, Pt/MXene-based flexible wearable non-enzymatic electrochemical sensor for continuous glucose detection in sweat, *ACS Appl. Mater. Interfaces*, 2023, **15**, 13290–13298.
- 33 S. Guenneau and T. Puvirajesinghe, Fick's second law transformed: one path to cloaking in mass diffusion, *J. R. Soc., Interface*, 2013, **10**, 20130106.
- 34 X. Sun, M. Zhang, J. Chang, L. Xie, Q. Ren, W. Jiang, *et al.*, Ti<sub>3</sub>C<sub>2</sub>Tx@ Pt nanocomposite based colorimetric and electrochemical dual-mode platform for glucose detection, *Sens. Biosens. Res.*, 2025, 100800.
- 35 A. R. Tzafirri, Michaelis-Menten kinetics at high enzyme concentrations, *Bull. Math. Biol.*, 2003, **65**, 1111–1129.
- 36 S. S. Datwani and K. J. Stebe, The dynamic adsorption of charged amphiphiles: The evolution of the surface concentration, surface potential, and surface tension, *J. Colloid Interface Sci.*, 1999, **219**, 282–297.
- 37 J. Xue, J. Li, Y. Ma, E. A. Obaid, H. Ouyang, T. Guo, *et al.*, Multivalent Pt/Ti<sub>3</sub>C<sub>2</sub>Tx nanocomposite-based immunochromatographic sensor for colorimetric/temperature/pressure trimodal detection, *Anal. Chem.*, 2024, **96**, 15074–15080.
- 38 V. Thirumal, R. Yuvakkumar, P. S. Kumar, G. Ravi and D. Velauthapillai, Facile preparation and characterization of MXene@ Platinum nanocomposite for energy conversion applications, *Fuel*, 2022, **317**, 123493.
- 39 L.-X. Li, G.-C. Zhang, W.-J. Sun, H.-Y. Zhang, S.-X. Wang, J.-L. Wei, *et al.*, Construction of ultra-small Pt nanoparticles@ Ti<sub>3</sub>C<sub>2</sub>Tx MXene electrocatalyst for efficient and stable electrochemical hydrodechlorination of chloramphenicol, *Chem. Eng. J.*, 2022, **433**, 134415.
- 40 S. Schnell, Validity of the Michaelis–Menten equation–steady-state or reactant stationary assumption: that is the question, *FEBS J.*, 2014, **281**, 464–472.

